Improvement of thermal properties of ultra-high *Q* silicon microdisk resonators

Mohammad Soltani, Qing Li, Siva Yegnanarayanan and Ali Adibi

School of Electrical and Computer Engineering, Georgia Institute of Technology, 777 Atlantic Drive NW, Atlanta, GA 30332-0250
soltani@ece.gatech.edu

Abstract: We present a detailed study of the thermal properties of ultra-high quality factor (*Q*) microdisk resonators on silicon-on-insulator (SOI) platforms. We show that by preserving the buried oxide layer underneath the Si resonator and by adding a thin Si pedestal layer at the interface between the resonator and the oxide layer we can increase the overall thermal conductivity of the structure while the ultra-high *Q* property is preserved. This allows higher field intensities inside the resonator which are crucial for nonlinear optics applications.

OCIS codes: (130.3120) Integrated optics devices; (230.5750) Resonators

References and links

1. R. A. Soref and J. P. Lorenzo, "All-Silicon Active and Passive Guided-Wave Components for λ=1.3 and 1.6μm," IEEE J. Quantum Electron. **22,** 873-879 (1986).
2. G. T. Reed and A. P. Knights, *Silicon Photonics: An Introduction, (*John Wiley, West Sussex, 2004).
3. L. Pavesi and D. J. Lockwood, *Silicon Photonics, (*Springer-verlag, New York, 2004).
4. M. Lipson, "Guiding, Modulating and Emitting Light on Silicon- Challenges and Opportunities," J. Lightwave Technol. **23**, 4222-4238 (2005).
5. S. F. Preble, Q. Xu, B. S. Schmidt, and M. Lipson, "Ultrafast all-optical modulation on a silicon chip," Opt. Lett. **30,** 2891–2893 (2005).
6. V. R. Almeida, C. A. Barrios, R. R. Panepucci, and M. Lipson, "All-optical control of light on a silicon chip," Nature **431**, 1081–1084 (2004).
7. A. Liu, R. Jones, L. Liao, D. Samara-Rubio, D. Rubin, O. Cohen, R. Nicolaescu, and M. Paniccia, "A high-speed silicon optical modulator based on a metal-oxide-semiconductor capacitor," Nature **427**, 615–618 (2004).
8. L. Zhou and A. W. Poon, "Silicon electro-optic modulators using p-i-n diodes embedded 10-micron-diameter microdisk resonators," Opt. Express **14**, 6851-6857 (2006).
9. H. Rong, R. Jones, A. Liu, O. Cohen, D. Hak, A. Fang, and M. Paniccia, "A continuous-wave Raman silicon laser," Nature **433**, 725–728 (2005).
10. K. Vahala, *Optical microcavities*, (World Scientific, Singapore, 2004).
11. T. Asano, B. S. Song, and S. Noda, "Analysis of the experimental *Q* factors (~ 1 million) of photonic crystal nanocavities," Opt. Express **14**, 1996-2002 (2006).
12. M. Borselli, T. J. Johnson, and O. Painter, "Beyond the Rayleigh scattering limit in high-*Q* silicon microdisks: theory and experiment," Opt. Express **13,** 1515–1530 (2005).
13. M. Soltani, S. Yegnanarayanan, and A. Adibi, "Ultra-high *Q* planar silicon microdisk resonators for Chip-Scale Silicon Photonics," Opt. Express **15**, 4694-4704 (2007).
14. T. J. Johnson, M. Borselli, and O. Painter, "Self-induced optical modulation of the transmission through a high-*Q* silicon microdisk resonator," Opt. Express **14**, 817-831(2006).
15. P. Barclay, K. Srinivasan, and O. Painter, "Nonlinear response of silicon photonic crystal microresonators excited via an integrated waveguide and fiber taper," Opt. Express **13**, 801-820 (2005).
16. T. Carmon, L. Yang, and K. J. Vahala, "Dynamical thermal behavior and thermal self stability of microcavities," Opt. Express **12**, 4742-4750 (2004).

#88647 - $15.00 USD Received 16 Oct 2007; revised 17 Nov 2007; accepted 17 Nov 2007; published 10 Dec 2007

17. G. Priem, P. Dumon,W. Bogaerts, D. Van Thourhout, G. Morthier, and R. Baets, "Optical bistability and pulsating behaviour in Silicon-On-Insulator ring resonator structures," Opt. Express **13**, 9623-9628 (2005).
18. C. Manolatou, M. J. Khan, S. Fan, P. R. Villeneuve, H. A. Haus, J. D. Joannopoulos, "Coupling of modes analysis of resonant channel add-drop filtering," IEEE J. Lightwave Technol. **35**, 1322-1331 (1999).

1. Introduction

The quest for the integration of optical functionalities in silicon-on-insulator (SOI) platform is emerging into new directions to bring photonics and electronics in a monolithic chip [1-4]. A variety of Si-based optical components has shown promising compatibilities with SOI technology, which is also the host for CMOS electronics [5-9]. Among the optical components, microresonators have had a large impact on different applications such as filtering, sensing, delay, and enhancement of light-matter interactions [10]. Recent advances in the design and improvements in the fabrication of Si-based microresonators have demonstrated cavities with quality factors (*Q*s) above 1 million in both standing wave resonator (e.g. photonic crystal cavity [11]), and traveling wave resonator (TWR) (e.g. microdisk resonator [12,13]) architectures. High *Q* and low electromagnetic mode volume of these resonators can build up a strong electromagnetic field inside them, even at low optical powers. As a result, strong interaction of electromagnetic field with the material (Si in this case) can occur inside the resonator [14, 15]. This may proceed to nonlinear effects such as two photons absorption (TPA) which accordingly generates a large number of free carriers (FC) inside the resonator [14]. The effect of these free carriers on the properties of the microresonators are: 1) Mode energy of the resonator can be absorbed and converted into heat energy which accordingly degrades the *Q*. 2) The resonator temperature rises up due to the generated heat which consequently changes the refractive index of the resonator in the positive direction. Hence, a thermally induced linewidth broadening occurs in the spectrum of the resonator [14-16]. 3) Refractive index of the resonator changes in the negative direction due to the free carrier dispersion effect [14], thereby, a blue shift in the resonance frequency of the resonator occurs.

Hence, increasing the optical power, in a lot of high *Q* resonator applications, can degrade the performance and sensitivity of the device due to the linewidth broadening. Therefore, the structure of the resonator should be functionalized or modified to suppress or at least minimize these non-idealities on the spectral response of the resonator.

In most of the recent reports on Si microresonators, the oxide substrate underneath the resonator is removed to guarantee obtaining an ultra-high *Q* [11, 12, 14, 15]. The main disadvantage of this substrate removal is that the cavity structure becomes thermally isolated from the underneath Si layer. Accordingly, the effective thermal conductivity of the resonator becomes very small [12], resulting in big rise of the temperature. In the case of an undercut microdisk resonator [12], the existence of a narrow oxide micropost for holding the microdisk on the underneath Si bulk layer is not too effective in reducing the temperature as it is far from the active region that energy mode profile of the resonator and consequently the peak temperature rise exist. This results in a large thermal resistance from the active microdisk cavity to the underneath Si bulk layer which results in thermal broadening, bistability, and other unwanted effects as we increase the input optical power impinging on the microdisk cavity [14, 15].

In a recent work, we performed a detailed theoretical and experimental study on the impact of the oxide substrate on the *Q* of the Si microdisk structures, and we showed that substrate is not a main factor in limiting the *Q*. In fact, experimental values of more than 1 million for the *Q* of a Si microdisk on substrate were achievable [13]. Hence, preserving the oxide layer underneath the resonator, besides preserving the ultra-high *Q* properties, provides

#88647 - $15.00 USD Received 16 Oct 2007; revised 17 Nov 2007; accepted 17 Nov 2007; published 10 Dec 2007

a larger heat sink area to transfer the heat away from the resonator, and therefore, to improve the net thermal conductivity of the structure. Consequently, when the SiO_2 layer is preserved, non-idealities due to thermal effects are significantly reduced even at high optical powers,

In this paper, we report a detailed quantitative study of the effect of the SiO_2 substrate on improving the thermal conductivity of microdisk resonators on SOI platform, and the results are compared with the ones for the undercut microdisk structures. Experimental evidence for the effect of high power on the linewidth of the microdisk structure is presented in section 2. A general model for the thermal broadening of the cavity linewidth is described in section 3, and its application to the thermal analysis of microdisk resonators is explained in section 4. The simulation results for the detailed comparison of thermal properties of Si microdisk resonators with and without the underneath SiO_2 layer is presented in section 5. Final conclusions are made in section 6.

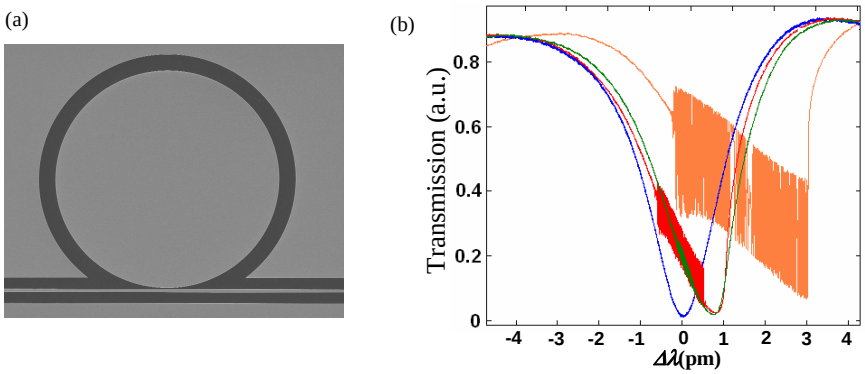

Fig. 1. (a) SEM image of a Si microdisk resonator with radius 20μm and thickness 250nm coupled to a waveguide with the width 550 nm. (b) The resonance spectrum of one of the microdisk modes at the critical coupling regime for different values of input optical power. The blue curve and the orange curve correspond to the lowest power and the highest power, respectively. By increasing the power, thermally-induced linewidth broadening as well as oscillation appears in the spectrum. The input power from the laser source for these four cases is 100μW: blue, 1.1mW: green, 1.6mW: red, 2.4mW: orange and the insertion loss of the waveguide is about 25 dB. The unloaded Q of this resonance mode is Q_0~1.2x10^6.

2. Experimental results

In order to observe the thermal non-idealities at high powers in Si microresonators, we fabricated an ultra-high Q microdisk and characterized its spectrum at different levels of input power. In Fig. 1(a) the scanning electron microscope (SEM) image of a Si microdisk resonator with radius 20 μm and thickness 250 nm, coupled to a waveguide with a width of 550 nm is shown. The spacing between the waveguide and the resonator is 200 nm. A shallow Si pedestal layer with a thickness of about 50nm is at the interface between the oxide layer and the microdisk. As will be discussed later, the presence of this layer improves the thermal conductivity of the structure in addition to enabling the integration of p-n junction next to the microresonator to remove the free carriers from the active region. The Q of this resonator was measured using the technique described in [13]. The details of the fabrication of this structure are explained in [13]. Figure 1(b) shows the spectrum of one of the resonance modes of this microdisk measured at different levels of input optical power in the waveguide. As seen from Fig. 1(b), the broadening of the spectrum is observed at higher powers, where the spectrum deviates from a Lorentzian shape and becomes asymmetric. As shown in Fig. 1(b), by orange curve, further increase in the optical power results in thermal-FC oscillations. This is a cycling dynamic between the blue shifting of the resonance due to TPA-induced FC generation, and red shifting of the resonance due to the temperature rise as a consequence of

#88647 - $15.00 USD Received 16 Oct 2007; revised 17 Nov 2007; accepted 17 Nov 2007; published 10 Dec 2007

FC absorption and heating generation. The detailed study of this self-induced optical oscillation phenomenon has been discussed in [14] and is not the scope of this paper.

3. A general model of thermal broadening of the resonator linewidth

As thoroughly discussed in [16], for a traveling wave resonator (TWR) such as a microdisk that is coupled to a waveguide, the heat generated inside the resonator can be expressed as follows:

$$\dot{q}_{in} = (\frac{Q}{Q_{abs}})\eta P \frac{1}{(\frac{\lambda_p - \lambda_r}{\Delta\lambda/2})^2 + 1} = P_h \frac{1}{\left(\frac{\lambda_p - \lambda_r}{\Delta\lambda/2}\right)^2 + 1} \quad (1)$$

$$P_h = P\eta\frac{Q}{Q_{abs}} \quad (2)$$

$$\lambda_r = \lambda_0(1 + a\Delta T) \quad (3)$$

In the above equations $\dot{q}_{in}$ is the rate of heat energy generated inside the resonator with respect to time; P is the light input power inside the waveguide; η is the energy coupling rate from the waveguide to the resonator; Q is the loaded resonator quality factor (due to the intrinsic quality factor of resonator (Q_0) and the loading effect by the waveguide), Q_{abs} is the cavity quality factor due to absorption of energy by FCs and converting it to heat generation; λ_p is the pump wavelength in the waveguide; λ_r is the resonator wavelength (which is temperature dependent); λ_0 and $\Delta\lambda$ are the resonance wavelength and linewidth of the cold resonator, respectively; ΔT is the temperature rise of the cavity; and a is thermal shift coefficient of the cavity resonance wavelength.

As discussed in [12,13], in ultra-high Q microdisk resonators, the light absorption by FCs (generated by the cavity light energy because of the presence of the electronic surface states at the surfaces of the Si resonator) is the main factor to limit the Q_0, and other effects such as surface scattering and radiation have a weak role in limiting the Q_0. Therefore, with a very good approximation, the intrinsic quality factor of the resonator (Q_0) is Q_{abs}. Consequently, in the critical coupling regime, $\eta = 2$, $Q \approx 0.5\, Q_{abs}$, and therefore, $P_h \approx P$.

The net heat, in the cavity, increases the cavity temperature as follows:

$$C_p\Delta\dot{T}(t) = \dot{q}_{in} - \dot{q}_{out} = \dot{q}_{in} - K\Delta T(t) \quad (4)$$

where C_p and K are the net constant-pressure specific heat capacity and the thermal conductivity of the resonator, respectively, and $\dot{q}_{out}$ is rate of the thermal energy flux that leaves the system, which is proportional to ΔT and K. Combining Eqs. (1)-(4) and assuming a steady state condition (i.e. $\Delta\dot{T}(t)=0$) we obtain the following:

$$0 = P_h \frac{1}{\left(\frac{\lambda_p - \lambda_r}{\Delta\lambda/2}\right)^2 + 1} - K(\frac{\lambda_r}{\lambda_0} - 1)/a \quad (5)$$

By solving Eq. (5) we can obtain the λ_r for different levels of input power and different values for the input light wavelength (λ_p). Correspondingly, the power transmission through the waveguide in the critical coupling regime can be obtained as follows [18]:

#88647 - $15.00 USD Received 16 Oct 2007; revised 17 Nov 2007; accepted 17 Nov 2007; published 10 Dec 2007

$$T = \left| \frac{j(\omega_p - \omega_r)}{j(\omega_p - \omega_r) + 1/\tau} \right|^2 = \left| \frac{j\dfrac{\lambda_p - \lambda_r}{\Delta\lambda/2}}{j\dfrac{\lambda_p - \lambda_r}{\Delta\lambda/2} + 1} \right|^2 \qquad \left(\tau = \frac{2Q}{\omega_r} = \frac{2\lambda_r}{\omega_r \Delta\lambda}\right) \tag{6}$$

where ω_p and ω_r are the pump and cavity frequencies, respectively, and τ is the lifetime of the loaded cavity.

Figure 2(a) shows the transmission through the waveguide for a wavelength range around the resonance (λ_0) at different input pump power levels (P). Increasing the input power can even make the transmission response into a bistable shape as shown by the orange curve in Fig. 2(a). In experiments, this bistability is observed by obtaining large transmission changes (or jumps, shown by dash lines in Fig. 2(a)) when the sweeping laser wavelength passes through the wavelengths corresponding to the edges of the bistability region. This fact is shown in Fig. 1(b), where the big jump in the orange curve corresponds to passing through one edge of the bistability region.

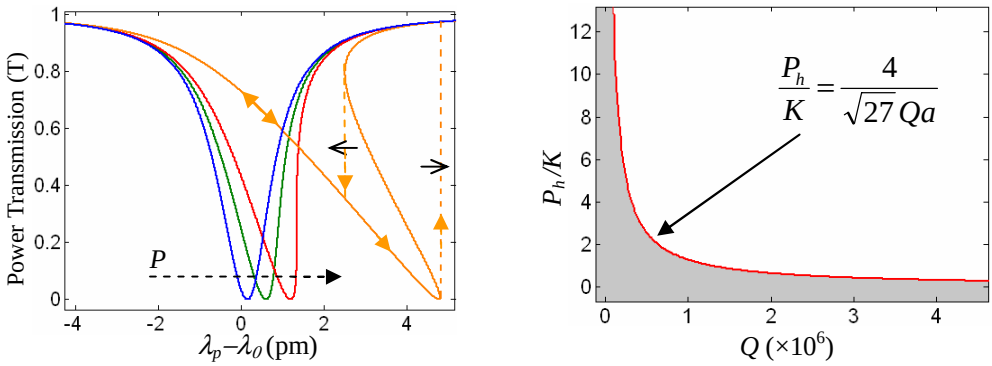

Fig. 2. (a). Transmission response of a coupled waveguide-resonator structure, with a loaded Q=10^6, in the critical coupling regime, at different levels of input optical power P=*[0.1, 0.33, 0.77, 3]K/Qa*, as shown by different colors (blue, green, red, and orange curves, respectively). At higher powers, besides broadening, the spectrum shows a bistable-type behavior, as shown by the orange curve. In experiments, a sharp transition in the transmission (as shown by dash lines) is observed at one of the edges of the bistability region depending on the direction of sweeping. (b) The threshold (red curve) to observe bistable behavior in the spectrum. No bistable behavior is observed in the shaded region.

Using Eq. (5), a threshold for the generated heat power (P_h) and accordingly the input power can be obtained below which the resonance spectrum dose not show a bistable shape. This threshold is obtained by solving Eq. (5) and applying the mathematical conditions to obtain λ_r as a one-to-one function of λ_p. Therefore, no bistability in λ_r and consequently in T is observed below this threshold. Figure 2(b) shows this threshold curve as a function of the loaded Q of the resonator. The shaded region in Fig. 2(b) corresponds to the conditions for Q, and P_h/K for which no bistable behavior is observed in the spectrum. In addition, moving far below the threshold reduces the broadening. In fact, as shown in Fig. 2(b), for larger thermal conductivities (K), larger optical power (P) can be coupled into the resonator while no bistability and less broadening is observed in the resonance spectrum. Moreover, for ultra-high Q cavities, the threshold power scales linearly as the thermal conductivity and an increase in thermal conductivity directly translates into a higher coupled power into the cavity, thereby enabling high-power and potentially nonlinear applications.

#88647 - $15.00 USD Received 16 Oct 2007; revised 17 Nov 2007; accepted 17 Nov 2007; published 10 Dec 2007

4. Thermal analysis of microdisk resonator

In the steady state condition the following heat equation can be considered for the simulation of the microdisk structure:

$$-\nabla.(K\nabla T) = Q_{th} \tag{7}$$

where K is the thermal conductivity of different materials used in the structures, and Q_{th} is the rate of heat energy generated in the structure. Considering the axial symmetry of the microdisk resonator, Eq. (7) can be analyzed more simply in the cylindrical coordinate. Note that the assumption of cylindrical symmetry is somehow approximate due to the presence of the coupling waveguide in the vicinity of the resonator. However, the effect of this waveguide-cavity coupling on the symmetry of the structure can be neglected due to the small interaction length. Therefore, T is assumed to have axial symmetry, and Eq. (7) can be represented in the cylindrical coordinate as follows:

$$-\frac{1}{r}\frac{\partial}{\partial r}(rK\frac{\partial T}{\partial r}) + \frac{m_T^2 KT}{r^2} - \frac{\partial}{\partial z}(K\frac{\partial T}{\partial z}) = Q_{th} \tag{8}$$

In Eq. (8), r and z are radial and axial coordinates respectively, and m_T is azimuthally harmonic number of temperature T in the microdisk resonator. As it will be explained below, m_T is in fact zero: For a Si microdisk, Q_{th} is proportional to the electric mode energy (proportional to |E|2, with E being the electric field inside the resonator) of the microdisk and electrical conductivity (σ) of Si as follows:

$$Q_{th} = \int_V \sigma \mid E \mid^2 \tag{9}$$

Although, at very higher powers, due to the TPA-induced FCs, σ and its spatial distribution becomes a function of the resonator mode energy, we can neglect this effect and consider a uniform conductivity for the resonator by assuming the power to be reasonably low. The electric field profile of the microdisk resonator with cylindrical symmetry can be represented in cylindrical symmetry as follows:

$$\overline{E} = \overline{E}(r,z)\exp(-im\phi) \tag{10}$$

Putting Eq. (10) into Eq. (9), it can be seen that no harmonic phase variation appears in Q_{th} and therefore, the distribution of Q_{th} is axially symmetric and monotonic. Therefore, the only available solution of Eq. (8) is for $m_T=0$ and the resulting heat equation is:

$$-\frac{1}{r}\frac{\partial}{\partial r}(rK\frac{\partial T}{\partial r}) - \frac{\partial}{\partial z}(K\frac{\partial T}{\partial z}) = Q_{th} \tag{11}$$

Eq. (11) can be solved for a given microdisk resonator to find the temperature distribution inside the structure. In this paper, we use an in-house finite element code for solving Eq. (11) in the COMSOL environment.

5. Simulation results

In order to assess the role of SiO_2 substrate and the shallow Si pedestal layer on the thermal conductivity of the microdisk resonator the following structures were considered for the analysis: (1) an undercut microdisk held by an oxide micropost (shown in Fig. 3(a)), and (2) a Si pedestal disk with the thicknesses of the pedestal layer (t) which is in general covered by either air or an oxide cladding (shown in Fig. 3(b)).

For the undercut disk, the radius and height of the underneath micropost oxide were 17μm and 1μm, respectively. Using a finite element technique as discussed in [13] the

#88647 - $15.00 USD Received 16 Oct 2007; revised 17 Nov 2007; accepted 17 Nov 2007; published 10 Dec 2007

electromagnetic mode profile of the structure is obtained. In this paper our focus is on the fundamental radial mode of the disk, although the final results for different modes regarding the thermal properties are similar. After finding the mode of the resonator, the generated heat energy that has a distribution proportional with the energy mode profile of the microdisk is incorporated into Eq. (11). Using a finite element method and applying the cylindrical symmetry conditions in the structure, the steady state temperature distributions of these structures can be obtained by solving Eq. (11). Figure 4(a) shows the temperature distribution for a typical pedestal microdisk with the dimensions given in the figure captions. As can be seen from Fig. 4(a), the peak temperature location coincides with the position of the maximum concentration of the electromagnetic energy, which is in the vicinity of the disk edge. A similar simulation can be performed for the undercut microdisk shown in Fig. 3(a). The results of these simulations show that the maximum temperature occurs when the electric field energy of the resonator mode is maximum (i.e. in the vicinity of the disk edge).

Based on the thermal conduction of the two structures shown in Fig. 3, it is expected that the undercut microdisk structure has the optical highest temperature rise at a given input power. To investigate this fact more quantitatively, we calculated the maximum temperature for both structures by solving Eq. (11).

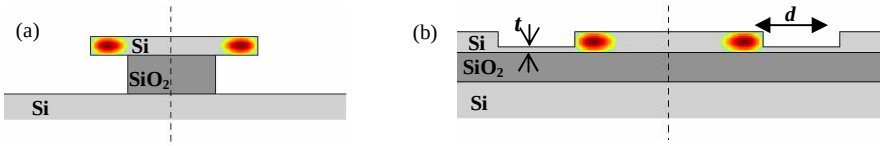

Fig. 3. (a). Cross section of an undercut Si microdisk resonator held by an oxide micropost on a Si bulk layer. (b) Cross section of a Si microdisk resonator on an oxide substrate. A shallow Si pedestal layer with thickness *t* is at the interface between the microdisk and the oxide layer. The etched region that separate the disk perimeter from the surrounding top silicon layer is *d*. In both (a) and (b) the cross section of the generated heat energy, which has a distribution proportional to that of the electromagnetic mode energy of the resonator, is shown.

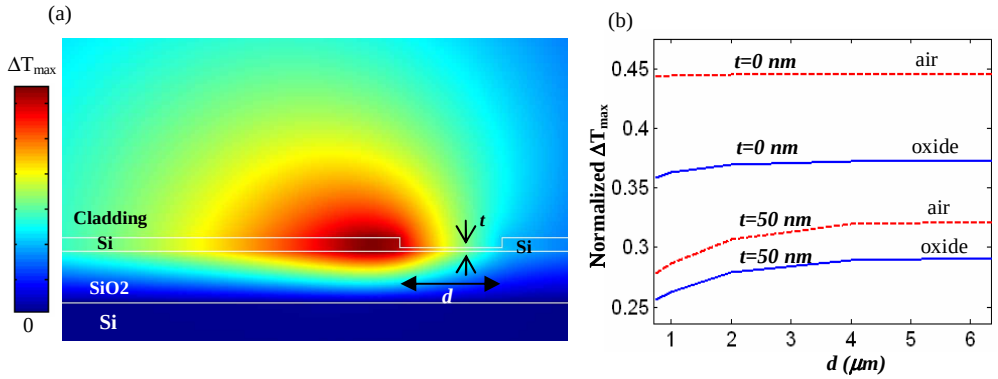

Fig. 4. (a). Cross section of the temperature distribution in a Si pedestal microdisk resonator on substrate; the disk radius and thickness are 20 μm and 250 *nm*, the Si pedestal thickness is 50 *nm*; and the oxide substrate thickness is 1μm. (b) The normalized peak temperature of the pedestal microdisk resonator with air and oxide claddings are also shown with dash and solid lines, respectively, for different value of *d*, which is the distance between the disk edge and the surrounding silicon layer. The temperatures are normalized to the peak temperature of the undercut microdisk under similar energy inside the microdisk resonators.

#88647 - $15.00 USD Received 16 Oct 2007; revised 17 Nov 2007; accepted 17 Nov 2007; published 10 Dec 2007

Figure 4(b) shows the normalized peak temperatures rise of the pedestal disk with air cladding and oxide cladding for pedestal thicknesses of *t=0* nm and *t=50* nm, respectively. As shown in this figure, the temperatures are normalized to the peak temperature rise of the undercut microdisk. These results show a dramatic reduction (over 3x) in the peak temperature (proportional to the thermal resistance), by using the pedestal microdisk architecture in comparison with undercut microdisk. For narrower micropost radii, the simulations confirmed that the peak temperature was dramatically growing for the undercut microdisk. From Fig. 4(b), it is observed that the pedestal microdisk with even an air cladding has a lower peak temperature when compared with the microdisk without the pedestal layer but covered with oxide cladding. In other words, the presence of the Si pedestal layer along with the underneath oxide layer has a major role in improving the overall thermal conductivity of the resonator. Our simulations were performed for different pedestal widths (*d*), which is the distance between the disk edge and the surrounding Si region. From Fig. 4(b), it is observed that the peak temperature rise increases with increasing *d* and eventually saturates at large *d*, due to the competition with the underneath substrate Si/oxide effects. Finally, the addition of the overall oxide cladding further improves the thermal conductivity as expected and shown in Fig. 4(b).

Thus, depending on the application and the level of optical power used in the actual experiments involving the Si microresonators, one can have different levels of thermal conductivity improvements by adding different layers (i.e., underneath SiO_2 layer, pedestal layer, and the oxide cladding layer) to the resonator. The simulations show that a thinner underneath oxide layer and a thicker Si pedestal layer result in a better thermal conductivity of the structure. However, the thicknesses of the underneath oxide and Si pedestal layers should be in a range to restrict the optical mode energy leakage of the microdisk to the underneath bulk Si layer and the surrounding, respectively, in order to preserve the ultra-high *Q* properties of the microdisk. In addition, with the presence of the cladding layer with an appropriate thickness, a metal heat sink layer can be deposited on top of the structure to extract larger heat energy from the structure without sacrificing the *Q* of the resonator. In fact, the cladding layer can be any other high quality optical material with a better thermal conductivity but with a refractive index much smaller than that of the resonator to preserve the ultra-high *Q* properties of the resonator. These issues and the corresponding design parameters are under more investigation.

6. Conclusion

We showed here that the thermal properties of high *Q* Si microresonators highly depend on the resonator structure. We showed that by preserving the oxide layer underneath Si in a microdisk resonator we can considerably improve the thermal conductivity of the structure without sacrificing *Q* (*Q*s above 10^6 are achievable with the oxide substrate and cladding layers present). We further showed that the presence of a shallow Si pedestal layer at the interface between the microdisk and the oxide layer further improves the thermal conductivity of the resonator by thermally connecting the Si disk to the surrounding Si region, thereby, suppressing the thermal instability issues at high optical powers while preserving the ultra-high *Q* property of the resonator.

Acknowledgments

This work was supported by Air Force Office of Scientific Research under Contract No. FA9550-06-01-2003 (G. Pomrenke).

#88647 - $15.00 USD Received 16 Oct 2007; revised 17 Nov 2007; accepted 17 Nov 2007; published 10 Dec 2007